IEEE Access
Multidisciplinary | Rapid Review | Open Access Journal

Received November 8, 2017, accepted December 19, 2017, date of publication January 1, 2018, date of current version March 9, 2018.

Digital Object Identifier 10.1109/ACCESS.2017.2788399

V2V Radio Channel Performance Based on Measurements in Ramp Scenarios at 5.9 GHz

CHANGZHEN LI[1], (Student Member, IEEE), KUN YANG[2], JUNYI YU[1], (Member, IEEE), FANG LI[1], YISHUI SHUI[3], FUXING CHANG[3], AND WEI CHEN[1], (Senior Member, IEEE)

[1]School of Automation, Wuhan University of Technology, Wuhan 430070, China
[2]Super Radio AS, 1208 Oslo, Norway
[3]School of Information Engineering, Wuhan University of Technology, Wuhan 430070, China

Corresponding author: Wei Chen (greatchen911119@suhu.com)

This work was supported in part by the Norwegian Research Council through the MAMIME Project under Grant 256309, in part by the Young Scientists Fund of the National Natural Science Foundation of China under Grant 61701356, and in part by the Fundamental Research Funds for the Central Universities under Grant 2017-JL-004.

ABSTRACT This paper focuses on vehicle-to-vehicle (V2V) radio channel properties under ramp scenarios with different structures. Ramps are categorized according to different construction structures into: 1) viaduct ramp with soundproof walls in an urban area and 2) a general ramp without soundproof walls in a suburban region. Furthermore, considering whether the line of sight is available, the entire propagation process of the radio signal is divided into various propagation zones. Propagation characteristics, including the distribution of fading, fading depth (FD), level crossing rate, average fade duration, Root-Mean-Square (rms) delay spread, propagation path loss, and shadow fading, have been estimated and extracted. In particular, the radio channel properties in different types of ramp scenarios are compared and some interesting findings are obtained: 1) an abrupt fluctuation of the received signal level (RSL) in the urban viaduct ramp scenario indicates the nonignorable impact of soundproof walls on V2V radio channel and 2) continuous changes of RSL and different FD values in various propagation zones can be observed in suburban ramp scenarios. Furthermore, the statistical characteristics of RMS delay spread are fitted using a generalized extreme value model with a good fit. Furthermore, propagation path loss is modeled, demonstrating the difference of path loss values in the transition region owing to the impact of soundproof walls. Overall, the research results emphasize the significance of the V2V radio channel modeling under ramp scenarios.

INDEX TERMS Vehicular communication, ramp scenarios, soundproof walls, channel properties.

I. INTRODUCTION

With the rapid development of the automobile industry, making traffic safe, efficient, and intelligent has become an inevitable trend. As an effective medium to exchange information, vehicle-to-vehicle (V2V) communication can effectively satisfy the application and service requirement of intelligent transportation systems (ITSs). Generally, two main aspects of vehicular communication are expected to serve modern transportation [1]–[5]. On the one hand, it can provide a stable network among vehicles to transmit smooth flow of information to fulfill the basic requirement of data exchange. On the other hand, it can offer support, including position location and collision avoidance, to improve traffic safety by sharing real-time data and revealing the changes of channel properties. Both applications highly depend on the quality of the radio channel, which varies with the propagation environment [1]–[3]. However, owing to the high speed and mobility of vehicles, vehicular communication requires a reliable and efficient wireless link to guarantee the stability and accuracy of real-time data. Moreover, the quality of the wireless communication link highly relies upon the properties of the radio channel, which are easily affected by the propagation environment [1]–[3]. Therefore, understanding V2V wireless propagation channels is important, especially under practical traffic environments.

A. LITERATURE REVIEW

The study of propagation channel characteristics of vehicular communication – both theoretical and practical – has previously attracted significant attention [1]–[3], [6]–[13]. Molisch *et al.* [1] provided an overview of numerous V2V channel measurement campaigns in many important traffic

2169-3536 © 2018 IEEE. Translations and content mining are permitted for academic research only.
Personal use is also permitted, but republication/redistribution requires IEEE permission.
See http://www.ieee.org/publications_standards/publications/rights/index.html for more information.

environments, and presented various classical channel properties, such as path loss, power delay profile (PDP), delay spread, and Doppler spread. The difference between vehicular communication and traditional cellular communication was demonstrated in this report as well. Paier *et al.* [14] carried out a car-to-car measurement campaign in a highway scenario. In this measurement, both measurement cars were traveling in opposite directions, and the results of path loss, PDP, and delay-Doppler spectra were studied and presented. References [7]–[9] and [15] are extensive studies devoted to V2V channel path loss modeling under various propagation conditions.

Furthermore, numerous research outcomes have not only addressed normal circumstances, such as urban areas [6]–[8], suburban areas [8], and highways [14] but also concentrated on particular scenarios. Theodorakopoulos *et al.* [16] derived a simulation model for a V2V radio channel in an urban cross-junction scenario, whereas Abbas *et al.* [17] deduced a flexible non-line-of-sight (NLOS) path loss model for a street intersection based on measurement. He *et al.* [10] studied V2V channel characteristics in different types of crossroad scenarios. Liu *et al.* [18] conducted measurement campaigns and determined the analytical results of V2V propagation path loss and RMS delay spread for overpass scenarios.

Moreover, a ramp, which is one among the multitudinous structures used in transportation, is also very common in V2V propagation environments. It usually appears together with a highway in suburban or rural areas [17], [19]. However, according to our investigation, in many large cities with heavy traffic, ramps are also common passageways for the urban high-speed viaducts used to ease the traffic pressure in the city. This structure of ramp will form NLOS area in the V2V propagation, which may obstruct the sight of the drivers, leading to traffic accident. Especially for the on ramp conditions. For example, there are at least 165 viaduct ramps on the Second Ring Road in Wuhan, China. V2V radio channel properties under this scenario have been studied preliminarily in [20], including PDP, RMS delay spread, and fading depth (FD). Li *et al.* [20] also focused on the impact of soundproof walls on vehicular communication under urban viaduct ramp scenarios.

B. CONTRIBUTIONS OF THIS PAPER

- **Measurement campaigns focusing on typical ramp scenarios are conducted.** We carried out four measurement campaigns in classical ramp cases to obtain V2V radio channel parameters. Two typical structures of ramps *i.e.*, viaduct ramp with soundproof walls in urban areas and a general ramp without soundproof walls in suburban regions (both on-ramp and off-ramp cases), are studied.
- **Small- and large-scale channel properties are estimated.** Based on the measurements, we analyzed V2V radio channel properties under typical ramp scenarios, including amplitude distribution, FD, level crossing rate (LCR), average fade duration (AFD), RMS delay spread, path loss, and shadow fading. The statistical distribution of measured RMS delay spread and shadowing are modeled using generalized extreme value (GEV) and Gaussian distribution, respectively.
- **Channel performance under different ramp scenarios is compared.** The comparisons and summarizations of the channel performance are carried out based on the classification of ramps. All the analysis results aim to illustrate valuable findings and serve the design and planning of vehicular communication systems.

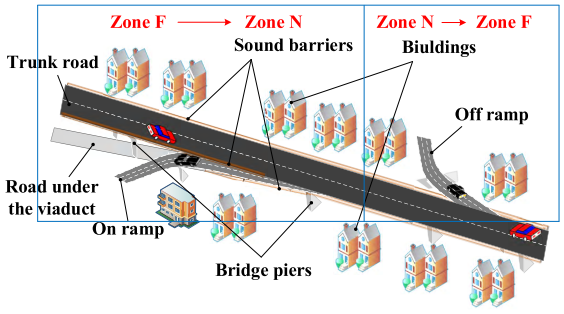

FIGURE 1. Sketch of urban viaduct ramp condition.

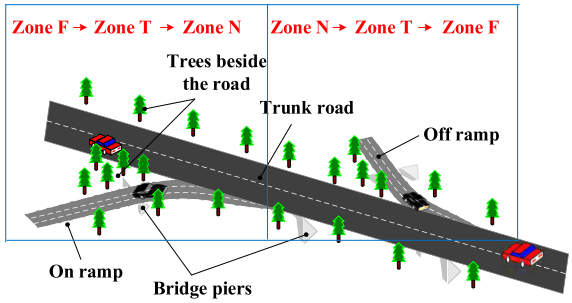

FIGURE 2. Sketch of general suburban ramps.

C. ORGANIZATION OF THE PAPER

In Section II, the types of ramps and main propagation zones in different periods are defined based on the typical structures and propagation conditions. Section III describes the measurement system and scenarios. The results of small-scale fading analysis are reported in Section IV, and the large-scale characteristics are investigated in Section V. Finally, the conclusions are presented in Section VI.

II. EXPECTED PROPAGATION MECHANISMS

Fig.1 and Fig.2 show the sketches of two typical ramp conditions. The ramp shown in Fig.1 appears usually in central city regions with an urban viaduct. As this is a special structure for transportation in dense urban areas, sound barriers are important to ensure that the normal and quiet lives of residents living near the road are not disturbed. Furthermore, a suburban general ramp is presented in Fig.2 in which trees rather than sound barriers exist between the trunk road and ramp. Some research results about the latter case were presented

in [17] and [19], whereas the former case will be investigated in the current study; further, the comparison between both cases will be emphasized. Considering the differences in the influence of ramp structures on V2V radio channels, the ramp scenarios in question can be classified into two types:

- **RSPW:** ramps with soundproof walls in urban viaduct scenario;
- **RnSPW:** ramps with trees instead of soundproof walls in a suburban area.

Furthermore, the entire process of driving a measurement vehicle through a ramp can be divided into various zones based on different propagation conditions.

- **Zone F:** In this zone, line of sight (LOS) is unavailable owing to the obstructions between the transmitter and receiver. It can be defined under two conditions in the current paper. For the **RSPW** case, it applies to the condition where Rx and Tx are separated by a soundproof wall, whereas for the **RnSPW** condition, it can be described as the area obstructed by trees beside the road.
- **Zone N:** This zone appears when both measurement cars are driving on the main road. Under this condition, LOS may be available. There are almost no obstructions between the transmitter and receiver, except other passing vehicles.
- **Zone T:** The existence of a long and high soundproof wall leads to NLOS region until LOS appears in the **RSPW** case. Nevertheless, the **RnSPW** condition is a relatively open area, and a transition process will alleviate the amplitude of variation. Thus, Zone T has practical significance only under the **RnSPW** condition.

In the following sections, we describe and analyze the V2V radio channel characteristics under the **RnSPW** and **RSPW** conditions. The differences among Zone F, Zone N, and Zone T will also be compared.

III. MEASUREMENT CAMPAIGNS

For the validation and analysis of the idea proposed in Section II, four measurement campaigns for the two typical ramp conditions mentioned above were carried out.

A. MEASUREMENT SYSTEM

The measurement system was composed of six parts: a Super Radio AS channel sounder with cables, transmitter (Tx), receiver (Rx), mobile vehicles, global positioning system (GPS), and computers. The channel sounder performed single-input single-output measurement and emitted a chirp signal. The carrier frequency was set to 5.9 GHz with a frequency bandwidth of 100 MHz. Tx and Rx were installed on the roof of measurement cars as shown in Fig.3(a) and Fig.3(b), respectively. In the **RnSPW** and **RSPW** measurements, omnidirectional antennas were used as Tx to transmit and as Rx to receive the chirp signal. Both omnidirectional antennas had vertical polarization with omnidirectional beam-width azimuth. Owing to the similar height of Tx and Rx as given in Table 1, the influence of beam-width elevation could be ignored. Further parameter

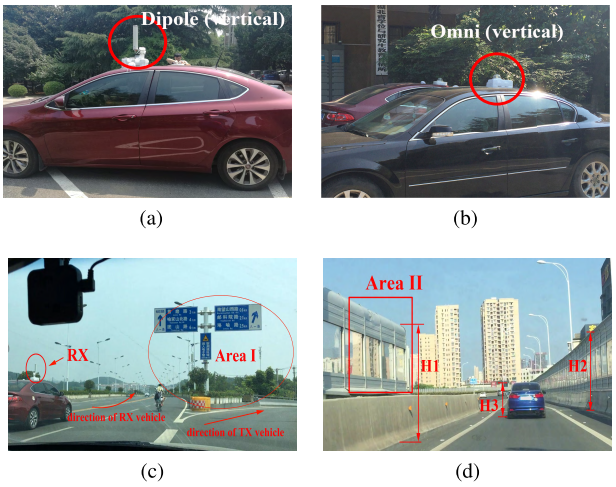

FIGURE 3. Installation of antennas and measurement scenarios. (a)(b) installation location of antennas, (c) the measurement ongoing picture of Scenario-I, which was taken from the view of Tx car, (d) view of the ramp with soundproof wall on the urban viaduct from Rx car in Scenario-IV.

TABLE 1. Measurement parameters.

Parameters	RnSPW	RSPW
Center frequency	5.9 [GHz]	5.9 [GHz]
Bandwidth	100 [MHz]	100 [MHz]
Chirp number	1933 [per s]	1933 [per s]
Sample number	2560 [per CIR]	2560 [per CIR]
Transmit power	16 [dBm]	16 [dBm]
Tx polarization	Vertical	Vertical
TX beam-width (Az.)	Omni-directional	Omni-directional
Tx gain	2 [dBi]	2 [dBi]
Tx height	1.57 [m]	1.57 [m]
Rx polarization	Vertical	Vertical
RX beam-width (Az.)	Omni-directional	Omni-directional
Rx gain	10 [dBi]	2 [dBi]
Rx height	1.78 [m]	1.50 [m]

details are listed in Table 1. To compute the distance between two mobile terminals and to map the traveling track, GPS data were logged into a computer via the integrated GPS module. Additionally, videos were recorded during the entire measurement.

B. MEASUREMENT SCENARIOS

The 5.9-GHz V2V radio channel measurements were conducted in Wuhan, China (Optical Valley Bridge Road and Xiongchu Viaduct on the Second Ring Road). By considering the aforementioned conditions, the measurement scenarios are designed as follows:

Scenario-I: (30°31'51''N, 114°22'38''E) Off-ramp in **RnSPW** (Fig.4(a)). The Tx car left the main road and headed to Nanwang Mountain West Road, whereas the Rx car continued to drive on the main road. Both cars were moving at the speed of 36-46 km/h.

Scenario-II: (30°31'53''N, 114°22'42''E) On-ramp in **RnSPW** (Fig.4(b)). The Tx car moved to Optical Valley

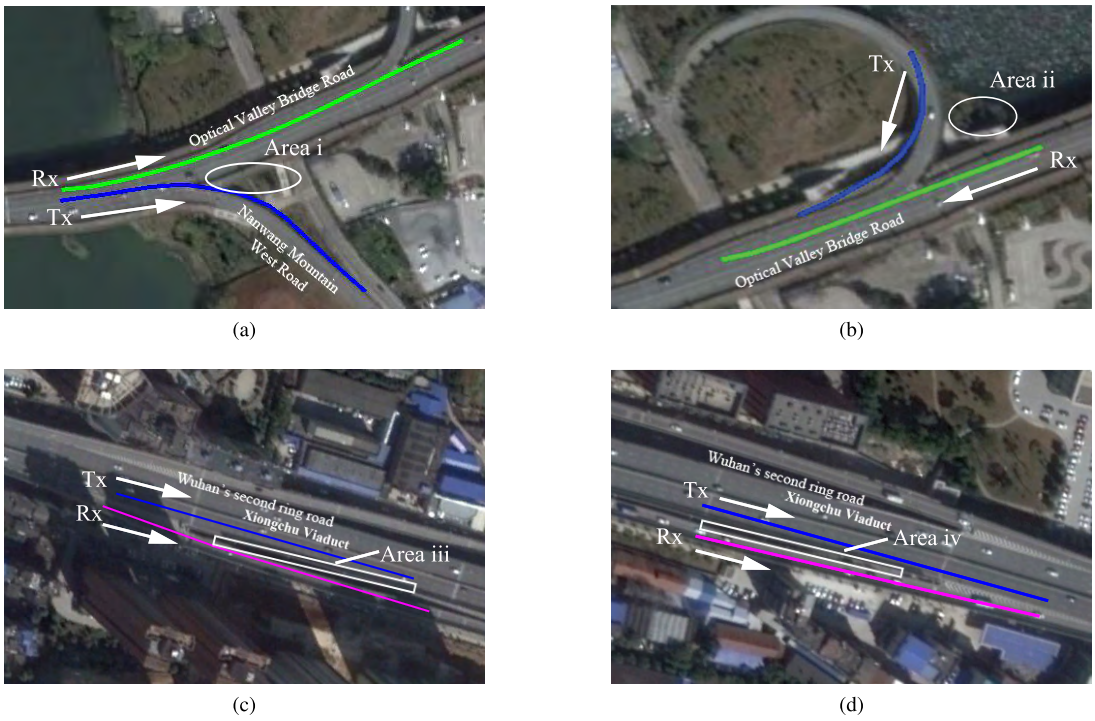

FIGURE 4. Images and travelling tracks of four measured scenarios in Wuhan. (a) Tx car drives out from the main road and Rx car continues moving on the main road; (b) Tx car enters the main road while Rx car is approaching the merging point on the main road; (c) Rx car turns off the viaduct and Tx car is still driving on the viaduct; (d) Rx car is driving into the viaduct along the entrance ramp when Tx car is approaching the merging point on the viaduct. (a)(b) are measured on Optical Valley Bridge and (c)(d) are carried out on Xiongchu Viaduct. White arrows show the driving direction of vehicles.

Bridge Road through the entrance ramp, whereas the Rx car passed the merging point on the main road. The speed of Tx was 19-23 km/h, whereas that of Rx was 74-83.5 km/h.

Scenario-III: (30°31'18''N, 114°19'4''E) Off-ramp in **RSPW** (Fig.4(c)). In this measurement, the Rx vehicle exited the Xiongchu viaduct on Wuhan's Second Ring Road and the Tx vehicle was still driving on the viaduct. There was a soundproof wall between the main road and ramp, whose height was much higher than that of the cars. Both measurement cars were moving at the speed of 64-76 km/h.

Scenario-IV: (30°31'11''N, 114°19'31''E) On-ramp in **RSPW** (Fig.4(d)). The Rx vehicle entered the viaduct through the entrance ramp whereas the Tx car was driving on the Second Ring Road. Both measurement vehicles arrived at the merging point at approximately the same time. A soundproof wall with a similar structure as the one in Scenario-III existed between the two passageways. The speeds of Tx and Rx were 26-44 km/h and 56-60 km/h, respectively.

Images of the four measurement campaigns are shown in Fig.4. Scenario-I and Scenario-II (**RnSPW**) are typical suburban environments, corresponding to the aforementioned sketch in Fig.2. In these cases, trees and road signs between the ramp and trunk road are the main scatterers, shown as Area i and Area ii in Fig.4, and marked as Area I in Fig.3(c). Scenario-III and Scenario-IV (**RSPW**) are urban areas. Soundproof walls with a large height (Area II in Fig.3(d)) have a significant impact on the properties of the V2V radio channel. Correspondingly, Area iii and Area iv show the relative location between the road and soundproof walls in Fig.4.

IV. SMALL SCALE CHARACTERISTICS

To ensure that the wide-sense stationary uncorrelated scattering assumption [21], [22] was established, a window of 10 wavelengths was utilized to remove the large-scale fading effect from the raw measured data. The maximum speed of the vehicles was utilized to set the window length to ensure that the sample number was sufficiently large (I-194299, II-108409, III-118855, IV-151943) such that the statistical results were reliable.

A. BEST FIT DISTRIBUTION OF FADES

Lognormal, Rayleigh, Rician, Nakagami-m, and Weibull distributions are widely used in mobile radio channel modeling [21], [23], [24]. However, there are variations of fitting results among various probability density functions (PDFs) under different propagation conditions. Thus, it is important to select an optimal model among them.

Akaike information criteria (AIC) [25] can evaluate the goodness-of-fit (GoF) between the statistical models and raw data. It has been used extensively in the selection of the appropriate fitting distribution [23], [26]–[29]. We employed it to select an optimal model in the current paper.

$$AIC_i = -2\sum_{n=1}^{N} ln\left[PDF_{\hat{\theta}_i}(x_n)\right] + 2D \tag{1}$$

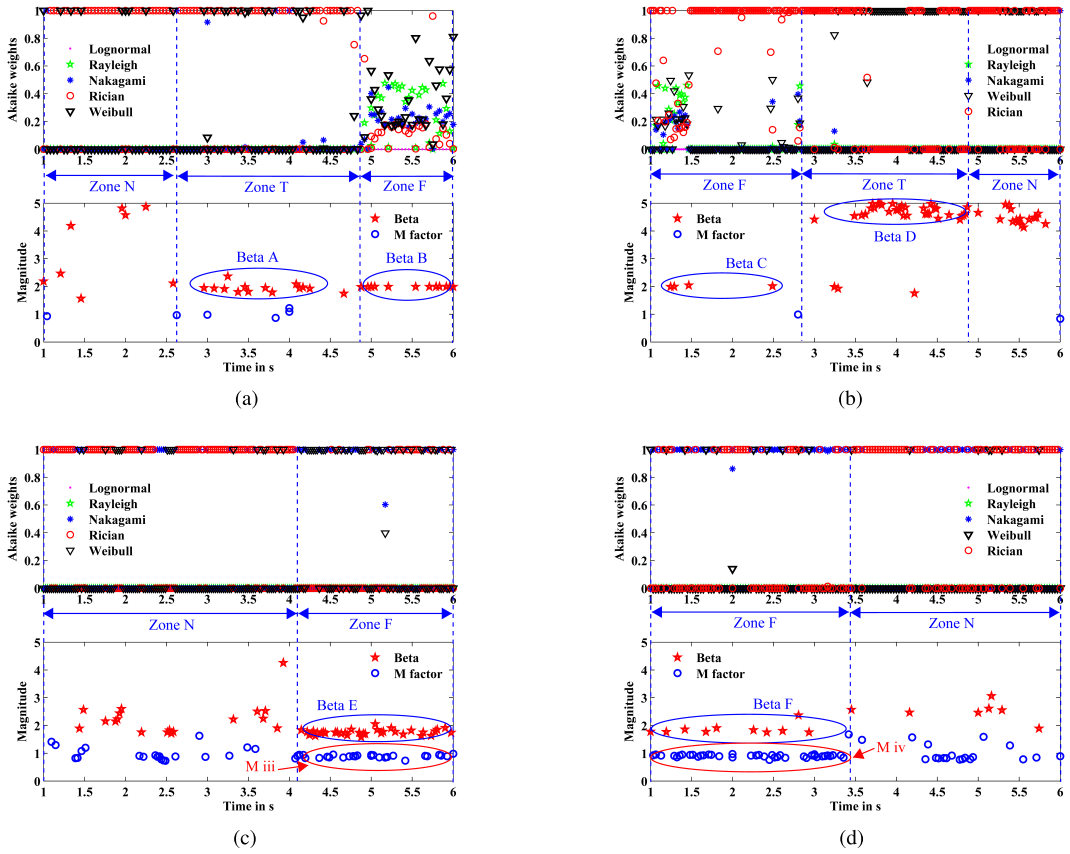

FIGURE 5. Akaike weights, partial shape parameters (β) of Weibull distribution and m-factors of Nakagami-m distribution for four series of measurement data. (a) Scenario-I. (b) Scenario-II. (c) Scenario-III. (d) Scenario-IV.

In Equation (1), PDF(x_n) and θ_i are the PDF and distribution parameter vector of the measurement data with the length of N, respectively. Further, $\hat{\theta}_i$ represents the maximum likelihood estimate of θ_i with the dimension D.

For convenience, Akaike weight w_i [26] defined by Equation (2) is usually viewed as a reference value for selecting a better fit. The total value of all w_i is 1, and a higher value of w_i provides a better distribution fit.

$$w_i = \frac{e^{\frac{-\Phi_i}{2}}}{\sum_{j=1}^{I} e^{\frac{-\Phi_j}{2}}} \tag{2}$$

where I is the total number of candidate distributions and $\Phi_i = AIC_i - \min_j(AIC_j)$ is the AIC difference.

Akaike weights are plotted in Fig.5, and the corresponding rates of small-scale fit distributions for each measured scenario are listed in Table 2. It is observed that, in Zone F, Rayleigh distribution reaches 43.75% in **Scenario-I** and 12.64% in **Scenario-II**, whereas the proportion of Rician distribution shows an absolute advantage in Zone N, with 75% and 65.31%, respectively, for Scenario-I and Scenario-II. In **Scenario-III** and **Scenario-IV**, the performance of Rician distribution in Zone N is similar to the observation in the previous two scenarios, *i.e.*, 70.31% and 67.47%, respectively. However, Weibull distribution and Nakagami-m distribution are outstanding in Zone F, with sum values of 76.83% and 64.94%, respectively, for Scenario-III and Scenario-IV.

Notably, in **Scenario-I** and **Scenario-II**, the performance of Rayleigh distribution in NLOS regions is consistent with the theoretical prediction in [21]. Furthermore, the Weibull or Nakagami-m distribution accounts for a large proportion of the fitting results of Zone F in **Scenario-III** and **Scenario-IV**. In order to explain this phenomenon further, the shape parameters (β) [30] of Weibull distribution and m-factors [31] of Nakagami-m distribution are plotted in Fig.5. Further, their mean values and standard deviations are listed in Table 2. It is observed that the shape parameters in Zone F (*Beta-B, Beta-C, Beta-E, and Beta-F* in Fig.5) are approximately 2 with a small standard deviation (0.06, 0.02, 0.09, and 0.19) and the m-factors are approximately 1, which illustrates that the distribution in this zone is close to Rayleigh distribution [21]. This is consistent with the expected performance in Zone F owing to the non-availability of LOS as it is blocked by trees in **Scenario-I, Scenario-II** and soundproof walls in **Scenario-III, Scenario-IV**. Further details of β and m-factor are given in Table 2.

From Fig.5 and Table 2, we can observe that the best-fit distribution varies with the change in the propagation condition. In the **RnSPW** case, the following were observed: (1) NLOS between Rx and Tx leads to the presence of Rayleigh channel; (2) Weibull distribution with shape

TABLE 2. Analysis results of each measured scenario.

Region	Parameters		Scenario-I	Scenario-II	Scenario-III	Scenario-IV
Zone N	Rate of the Small-Scale Best Fit Distribution	Lognormal	0	0	0	0
		Rayleigh	0	0	0	0
		Rician	75%	65.31%	70.31%	67.47%
		Nakagami-m	2.5%	2.04%	15.63%	24.10%
		Weibull	22.5%	32.65%	14.06%	8.43%
	Results of Fade Depth (dB)	Max.Fading Value	-9.34	-3.60	-7.36	-3.07
		1%	-7.88	-2.49	-2.38	-1.37
		50%	-0.10	-0.05	-0.03	0.04
		Fading Depth	7.78	2.44	2.35	1.41
		Max. Fading Depth	9.25	3.55	7.34	3.11
	Mean/Standard deviation of Beta (β)		3.58/1.48	4.49/0.24	2.25/0.59	2.51/0.34
	Mean/Standard deviation of m-factor		0.93/0	0.83/0	1.00/0.24	1.02/0.32
	Mean of Received Signal Level (dB)		-75.24	-73.54	-74.92	-67.73
Zone T	Rate of the Small-Scale Best Fit Distribution	Lognormal	0	0	-	-
		Rayleigh	0	0	-	-
		Rician	64.91%	53.19%	-	-
		Nakagami-m	8.77%	0	-	-
		Weibull	26.32%	46.81%	-	-
	Results of Fade Depth (dB)	Max.Fading Value	-6.01	-5.20	-	-
		1%	-4.96	-2.68	-	-
		50%	-0.32	-0.01	-	-
		Fading Depth	4.64	2.67	-	-
		Max. Fading Depth	5.69	5.19	-	-
	Mean/Standard deviation of Beta (β)		1.94/0.15	4.63/0.80	-/-	-/-
	Mean/Standard deviation of m-factor		1.02/0.13	-/-	-/-	-/-
	Mean of Received Signal Level (dB)		-84.39	-77.30	-	-
Zone F	Rate of the Small-Scale Best Fit Distribution	Lognormal	0	0	0	0
		Rayleigh	43.75%	12.64%	0	0
		Rician	6.25%	81.61%	23.17%	35.06%
		Nakagami-m	0%	1.15%	34.15%	51.95%
		Weibull	50%	4.60%	42.68%	12.99%
	Results of Fade Depth (dB)	Max.Fading Value	-1.18	-2.55	-7.21	-6.83
		1%	-0.97	-1.79	-4.69	-4.56
		50%	-0.02	-0.02	-0.23	-0.13
		Fading Depth	0.95	1.77	4.46	4.43
		Max. Fading Depth	1.16	2.53	6.98	6.70
	Mean/Standard deviation of Beta (β)		1.97/0.06	2.01/0.02	1.75/0.09	1.86/0.19
	Mean/Standard deviation of m-factor		-/-	0.99/0	0.89/0.05	0.90/0.04
	Mean of Received Signal Level (dB)		-91.44	-89.18	-87.29	-76.53

parameters (β) of approximately 2 and Nakagami-m distribution with m-factor of approximately 1 are observed with the change in the propagation environment; and (3) Rician distribution dominates in the LOS condition. However, in the **RSPW** case, the following were observed: (1) Weibull distribution and Nakagami-m distribution appear centrally in the block region caused by the soundproof wall; and (2) when the measurement cars move out of the blocked area, Rician distribution becomes the best fitting model.

B. RMS DELAY SPREAD

As the second central moment of PDP, RMS delay spread can provide a compact description of the delay dispersion of the radio channel [1], [22], [32]. A threshold is normally set to avoid influence from spurious components. According to [33], we set the threshold to 6 dB above the average noise floor in our analysis.

Fig.6(a) illustrates the statistical properties of RMS delay spread by using cumulative distribution functions (CDFs), whereas the corresponding PDFs are shown in Fig.6(b) to (e). From Fig.6(a), it can be observed that 90% RMS delay spread is within 39.37 ns, 42.74 ns, 145.8 ns, and 86.92 ns for Scenario-I, Scenario-II, Scenario-III, and Scenario-IV, respectively. The larger values in **Scenario-III** and **Scenario-IV** indicate that the reflections from the surroundings are richer than those in **Scenario-I** and **Scenario-II**. This is consistent with the relative openness of **Scenario-I** and **Scenario-II**, whereas the other two cases are not open owing to soundproof walls on the sides of the road.

Generally, the statistical characteristics of the RMS delay spread can be fitted well using a lognormal distribution [1], [34], [35]. However, from Fig.6, it is observed that the RMS delay spread in the current study is affected heavily by extreme values. To address the impact of extreme values of

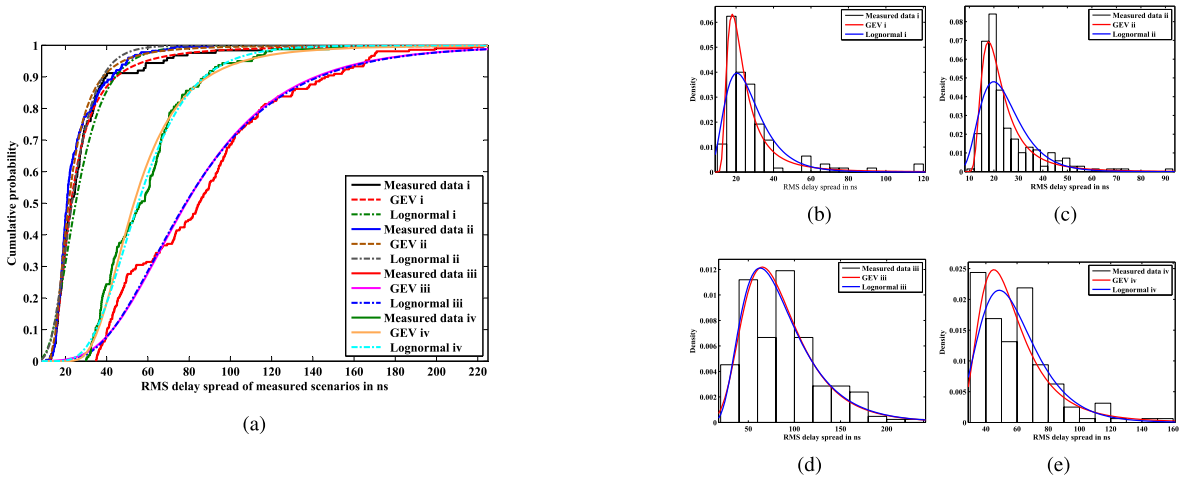

FIGURE 6. CDF and PDF of measured RMS delay spread, fitted models with GEV and Lognormal distribution. (a) CDFs and fitted curves, (b)-(e) PDFs and fitted curves for Scenario-I, Scenario-II, Scenario-III, and Scenario-IV, respectively. (a) CDF of RMS delay spread and fitted curves. (b) Scenario-I. (c) Scenario-II. (d) Scenario-III. (e) Scenario-IV.

TABLE 3. Parameters of GEV models and GoF of two models.

Cases	Case-I	Case-II	Case-III	Case-IV
k	0.4414	0.3368	0.0739	0.1763
σ (ns)	6.3408	5.5879	30.2600	15.035
μ (ns)	20.1409	19.3290	67.3272	47.5061
GoF of GEV	0.0509	0.0701	0.1088	0.0993
GoF of Lognormal	0.1004	0.1468	0.1050	0.0775

RMS delay spread on the channel parameters, we use the GEV distribution [36] to model it, which employs extreme values (maxima or minima) in the sample data, as expressed in Equation (3):

$$F(\tau_{rms}; k, \sigma, \mu) = exp\left(-\left(1 + k\left(\tau_{rms} - \frac{\mu}{\sigma}\right)\right)^{1/k}\right) \quad (3)$$

where k, σ, and μ are the shape factor, scaling parameter, and location parameter, respectively. The parameters of the GEV distribution are presented in Table 3.

Among the GEV parameters, k governs the tail behavior of the distribution. σ and μ represent the dispersion and average of the extreme observations, respectively [37]. The results presented in Table 3 indicate that σ and μ of **Scenario-III** and **Scenario-IV** are larger than the corresponding values of **Scenario-I** and **Scenario-II**. This illustrates that the surrounding scatterers in the **RSPW** cases can have an even stronger impact on the V2V radio channel. Furthermore, the consistency between the measured CDF $F_m(\tau_{rms})$ and the fitted CDF $F_t(\tau_{rms})$ is shown in Fig.6(a). The Kolmogorov–Smirnov test (*K-S* test) is used as the GoF indicator [38] to quantify the fitting degree, as shown in Equation (4):

$$GoF = \sup_{\tau_{rms}} |F_m(\tau_{rms}) - F_t(\tau_{rms})| \quad (4)$$

where *sup* denotes the supremum and the significance level of $GoF \leq \gamma = 0.11$ indicates a good fit [39].

Table 3 lists the result of GoFs between the fitted data and measured data. It can be observed that GoFs obtained from the GEV model are less than those obtained from the lognormal model for **Scenario-I** and **Scenario-II**. However, GoFs from both fitted models are almost the same for the other two scenarios. This also indicates that the soundproof walls reduce the extreme influence from the surrounding scatterers.

C. FADING DEPTH

Using our wideband measurement, we first executed the transformation from wideband signal to an equivalent narrowband signal [40]. By removing the effects of large-scale fading using a window of 10 wavelengths, small-scale fading obtained from four measurements is shown in Fig.7. Among them, FD is a measure of the variation of channel energy about its local mean, which is defined as the difference between the 50% and 1% signal levels [23], [41]. Moreover, the maximum FD, which is the difference between the signal levels of the 50% signal level and the maximum fading values, can also be a reference value [23]. The 50% and 1% values can be obtained from the empirical CDF, and the maximum fading values have been marked as green circles (*FD a*∼*FD h*) in Fig.7.

The results of FD are summarized in Table 2. From the results, we can observe that the maximum FD is approximately 9 dB in Zone N for **Scenario-I**, and it is smaller in Zone T (6 dB) and Zone F (1 dB). In contrast, for **Scenario-IV**, the maximum FD in Zone F is larger than that in Zone N.

Notably, in **Scenario-I** and **Scenario-II**, passing vehicles and roadside trees are the main reflection and scattering components, which lead to the severity of V2V radio channel fading (*e.g., FD a* and *FD e*). Instead, compared with passing vehicles, soundproof walls contribute more to the severe small-scale fading under **RSPW** scenarios. The variation of

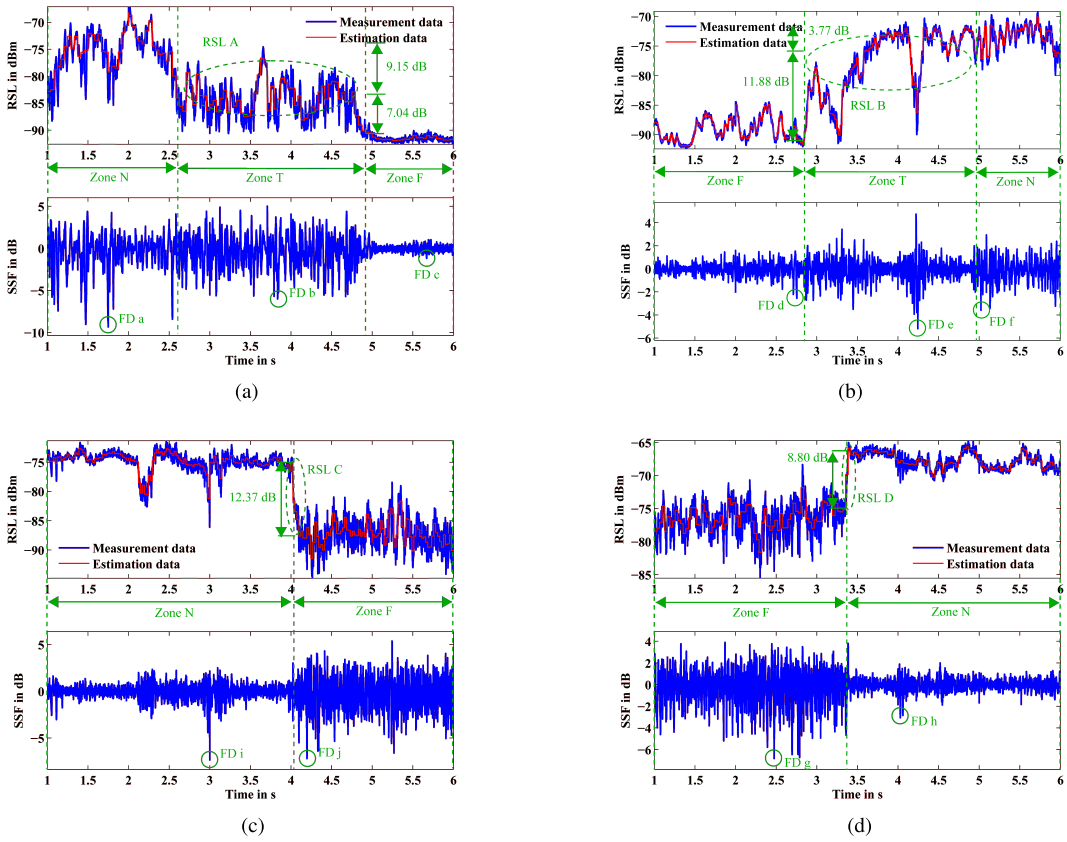

FIGURE 7. Measured results of each scenario: received signal level (and it without small-scale fading), small-scale fading. The green circles indicate the maximum fading values in each region. (a) Scenario-I. (b) Scenario-II. (c) Scenario-III. (d) Scenario-IV.

FD in each zone has been presented in Table 2, indicating that the reduction caused by passing vehicles, roadside trees, and soundproof walls cannot be neglected in the design of a V2V radio communication system.

D. LCR AND AFD

In addition to the characteristics mentioned previously, LCR and AFD are important for describing the statistics of mobile fading channels [21], [42]. Moreover, from a system point of view, extracting LCR and AFD related to a given threshold from the measurements is of wider significance. LCR denotes the frequency with which the received signal crosses (from down to up) a given threshold level per time unit; further, AFD determines the average duration for which the signal remains below a certain level [21]. In our research, the LCR values indicate the crossing times per window length (10λ), whereas AFD is also expressed in terms of the window length.

Fig.8 shows the measured LCR and AFD in Zone F in each scenario. To obtain a relatively complete description of the radio channel, we deduce LCR and AFD with respect to three typical threshold levels 0 dB, −2 dB, and −4 dB from the measured values. From the results listed in Table 4, it can be observed that, under similar driving environments and propagation conditions, LCR values are higher in **Scenario-III** and **Scenario-IV** than in **Scenario-I** and **Scenario-II** for the same threshold level. This is due to the influence of soundproof walls in the latter two scenarios. We can also draw a similar conclusion from the AFD curves. The comparison among these four measured scenarios shows that soundproof

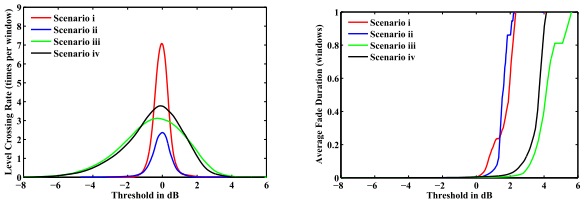

FIGURE 8. Level crossing rate and average fade duration in each Zone F. (a) LCR. (b) AFD.

TABLE 4. LCR values and AFD values of each measured scenario.

Scenarios		Case I	Case II	Case III	Case IV
LCR (times) per second	0 dB	7.05	2.36	3.07	3.76
	-2 dB	0	0.05	1.97	1.75
	-4 dB	-	0	0.58	0.51
AFD (second)	0 dB	0.0047	0.0026	0.0022	0.0047
	-2 dB	0	0.001	0.00089	0.0009
	-4 dB	-	0	0.00057	0.00052

walls in an urban viaduct environment can exacerbate the severity of V2V radio channel fading.

V. LARGE SCALE CHARACTERISTICS

A. PATH LOSS

Generally, path loss versus distance is used to describe the average attenuation of a radio signal caused by its propagation in the study of mobile communication [1], [22], calculated by Equation (5):

$$PL(dB) = P_t - P_r + G_t + G_r - L_0 \tag{5}$$

where P_t and P_r are the powers of Tx and Rx, respectively, G_t and G_r are the gains of their antennas, respectively. L_0 denotes the attenuation caused by the devices and cables. Propagation path loss is calculated by substituting the gain and power of antennas into Equation (5), and it is plotted in Fig.9.

Furthermore, we model path loss using the simple log-distance power law [22] based on Equation (6), which can predict the reliable communication range between Tx and Rx. The path loss versus log-distance curves are plotted in Fig.9.

$$PL_{law} = PL_0 + 10 \cdot n \cdot lg\left(\frac{d}{d_0}\right) + X_\sigma \tag{6}$$

where PL_{law} denotes the estimated path loss, d (extracted from the GPS data) is the distance between Tx and Rx, n is the path loss exponent estimated using linear regression, and X_σ is a zero-mean Gaussian distributed random variable with standard deviation σ. PL_0 is the path loss at a reference distance d_0 in dB. d_0 has been listed in Table 5. Only a few samples are available before d_0.

Fig.7 shows the received signal level (RSL) versus time for four measured scenarios. Different mean values of RSL can be observed in previously divided propagation zones, which are listed in detail in Table 2. For the same measured condition, we can observe that Rx received higher signal level in Zone N than in Zone T and Zone F. Moreover, for a clear comparison between **RSPW** and **RnSPW**, *RSL A, RSL B, RSL C,* and *RSL D* are marked with green circles in Fig.7. Notably, in the urban viaduct ramp scenario, an abrupt change (*RSL C, D*) without any buffer (such as *RSL A, B* in the other two scenarios) appears owing to the presence or absence of soundproof walls.

From Fig.9, it is observed that path loss values in the transition regions of **Scenario-III** and **Scenario-IV** are different from those in the transition regions of the other two scenarios (marked in red box in Fig.9). We also observe from Fig.9 that, for **Scenario-III** and **Scenario-IV**, path loss values change abruptly in the transition regions (at approximately 18.03 m and 43.32 m). However, they vary continuously in **Scenario-I** and **Scenario-II**. This observation is consistent with the discussion on the influence of soundproof walls in an urban viaduct environment. Furthermore, the value of n depends on the specific propagation environment. The lower the value, the better the propagation [8]. In these two types of ramp conditions, we derived the path loss exponent as

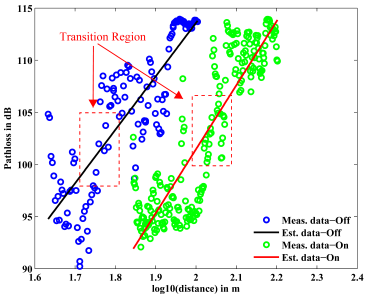

(a)

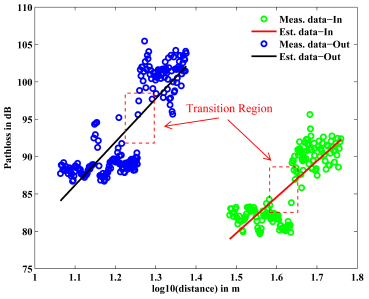

(b)

FIGURE 9. Measured and estimated path loss vs. distance. (a) Scenario-I, Scenario-II. (b) Scenario-III, Scenario-IV.

TABLE 5. Parameters of path loss model and shadowing.

Parameters	Case-I	Case-II	Case-III	Case-IV
d_0	46.50	72.97	12.82	32.69
n	5.126	6.136	5.777	4.822
σ^2	12.99	11.22	12.05	7.45
$p-value$	0.0270	0.0001	0.0023	0.0008

$n = 5.126$, 6.136, 5.777, and 4.822. They were larger than the obtained values of n under the urban condition in [8] ($n = 1.68$) and [43] ($n = 1.61$) and under suburban condition in [12] ($n = 2.5$). This illustrates that wireless propagation undergoes more attenuation under ramp scenarios.

B. SHADOW FADING

Shadow fading (X_σ) on a dB scale is commonly considered to follow a zero-mean Gaussian distribution with standard deviation (σ) related to the propagation environment [44]. We extracted shadowing values from four measured scenarios and fitted them with Gaussian distributions in Fig.10. Moreover, we obtained the p-values by using the K–S test to determine if shadowing extracted from the different cases follows the $N(0, \sigma^2)$ [45]. σ and p-values are given in Table 5. From the σ values, it can be observed that, for opening **Scenario-I** and **Scenario-II**, the σ values are slightly larger than in **Scenario-III** and **Scenario-IV**. This may be due to the shadowing effects of passing vehicles; however, the long soundproof wall results in a continuous shadow fading in **Scenario-III** and **Scenario-IV**. Furthermore, the small p-values indicate that the shadowing follows the $N(0, \sigma^2)$ well [45].

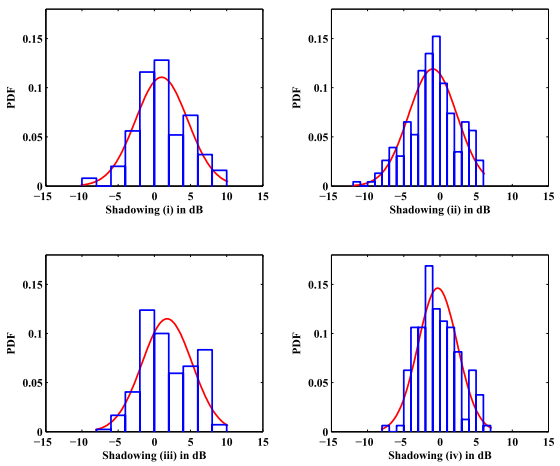

FIGURE 10. PDF of the shadowing for different propagation scenarios.

VI. CONCLUSION

This paper presented four V2V radio channel measurements conducted at 5.9 GHz under **RSPW** and **RnSPW** scenarios. The difference between the V2V radio channel properties of both cases was highlighted. Small- and large-scale characteristics under various propagation conditions were analyzed and compared. The main results of this paper are summarized as follows.

- **Small-scale characteristics.** By analyzing small-scale characteristics, we observed that Rician distribution offered the perfect fit when LOS was available under both RSPW and RnSPW scenarios. Rayleigh distribution performed best when LOS was unavailable in RnSPW; however, Weibull distribution with shape parameters of approximately 2 and Nakagami-m distribution with m-factor of approximately 1 fitted well under RSPW scenario. Owing to the heavy influence of extreme values, the GEV model provided a good match for the CDF and PDF of RMS delay spread. The FD of V2V radio channel under RnSPW scenario ranged from 2 dB to 7 dB, whereas it ranged from 2 dB to 4 dB in the RSPW case. Passing vehicles and roadside trees can lead to channel fading, and the fading varied with the propagation environment.
- **Large-scale characteristics.** The RSL fluctuated by 4∼12 dB owing to the impact of the change in propagation environment. Path loss could be modeled as a function of the log-distance using a simple power law with a path loss exponent of approximately 5. Further, abrupt changes were observed in path loss models under urban viaduct ramp scenarios owing to the influence of soundproof walls. The standard deviation values of shadow fading in the RnSPW case were slightly larger than those in the RSPW case owing to the effects of continuous passing vehicles.
- **Impact of different structures of ramps on V2V radio channel.** As the height of the soundproof wall was much higher than that of the vehicle, the impact of soundproof walls on the V2V radio channel properties in the RSPW case was evident. Compared with RnSPW, the transition process between LOS and NLOS cases was replaced by an abrupt change of channel properties in the RSPW case. Furthermore, the presence of soundproof walls could increase the FD and LCR.

The results of our work can serve as the basis for the design of V2V communication systems. In particular, they can be applied to the ITS to reduce urban traffic congestion and traffic accidents.

COMPETING INTERESTS

The authors declare that there are no conflicts of interest regarding the publication of this paper.

ACKNOWLEDGMENTS

The authors express their sincere gratitude to the Super Radio AS. and Ningbo Allmeas Tech. Co. Ltd., who supplied the measurement equipment, for their generous support. With their support, they could complete the measurement campaigns and other research works. They also appreciate the support of their friends and colleagues during the measurement campaigns.

REFERENCES

[1] A. F. Molisch, F. Tufvesson, J. Karedal, and C. F. Mecklenbrauker, "A survey on vehicle-to-vehicle propagation channels," *IEEE Wireless Commun.*, vol. 16, no. 6, pp. 12–22, Dec. 2009.

[2] H. Boeglen, B. Hilt, P. Lorenz, J. Ledy, and A.-M. Poussard "A survey of V2V channel modeling for VANET simulations," in *Proc. IEEE 8th Int. Conf. Wireless Demand Netw. Syst. Services (WONS)*, Jan. 2011, pp. 117–123.

[3] H. Hartenstein and L. P. Laberteaux, "A tutorial survey on vehicular ad hoc networks," *IEEE Commun. Mag.*, vol. 46, no. 6, pp. 164–171, Jun. 2008.

[4] C. B. Math, H. Li, and S. H. de Groot, "Risk assessment for traffic safety applications with V2V communications," in *Proc. IEEE 84th Veh. Technol. Conf. (VTC-Fall)*, Sep. 2016, pp. 1–6.

[5] P. Alexander, D. Haley, and A. Grant, "Cooperative intelligent transport systems: 5.9-GHz field trials," *Proc. IEEE*, vol. 99, no. 7, pp. 1213–1235, Jul. 2011.

[6] A. Roivainen, P. Jayasinghe, J. Meinila, V. Hovinen, and M. Latva-Aho, "Vehicle-to-vehicle radio channel characterization in urban environment at 2.3 GHz and 5.25 GHz," in *Proc. IEEE 25th Annu. Int. Symp. Pers., Indoor, Mobile Radio Commun. (PIMRC)*, Sep. 2014, pp. 63–67.

[7] Z. H. Mir and F. Filali, "Simulation and performance evaluation of vehicle-to-vehicle (V2V) propagation model in urban environment," in *Proc. IEEE 7th Int. Conf. Intell. Syst., Modelling Simulation (ISMS)*, Jan. 2016, pp. 394–399.

[8] O. Onubogu, K. Ziri-Castro, D. Jayalath, K. Ansari, and H. Suzuki, "Empirical vehicle-to-vehicle pathloss modeling in highway, sub-urban and urban environments at 5.8 GHz," in *Proc. IEEE 8th Int. Conf. Signal Process. Commun. Syst. (ICSPCS)*, Dec. 2014, pp. 1–6.

[9] T. Abbas, A. Thiel, T. Zemen, C. F. Mecklenbrauker, and F. Tufvesson, "Validation of a non-line-of-sight path-loss model for V2V communications at street intersections," in *Proc. IEEE 13th Int. Conf. ITS Telecommun. (ITST)*, Nov. 2013, pp. 198–203.

[10] R. He *et al.*, "Vehicle-to-vehicle radio channel characterization in cross-road scenarios," *IEEE Trans. Veh. Technol.*, vol. 65, no. 8, pp. 5850–5861, Aug. 2016.

[11] A. Paier *et al.*, "Characterization of vehicle-to-vehicle radio channels from measurements at 5.2 GHz," *Wireless Pers. Commun.*, vol. 50, no. 1, pp. 19–32, 2009.

[12] L. Cheng, B. E. Henty, D. D. Stancil, F. Bai, and P. Mudalige, "Mobile vehicle-to-vehicle narrow-band channel measurement and characterization of the 5.9 GHz dedicated short range communication (DSRC) frequency band," *IEEE J. Sel. Areas Commun.*, vol. 25, no. 8, pp. 1501–1516, Oct. 2007.

[13] S. Beygi, U. Mitra, and E. G. Ström, "Nested sparse approximation: Structured estimation of V2V channels using geometry-based stochastic channel model," *IEEE Trans. Signal Process.*, vol. 63, no. 18, pp. 4940–4955, Sep. 2015.

[14] A. Paier *et al.*, "Car-to-car radio channel measurements at 5 GHz: Pathloss, power-delay profile, and delay-Doppler spectrum," in *Proc. 4th Int. Symp. Wireless Commun. Syst. (ISWCS)*, Oct. 2007, pp. 224–228.

[15] J. Karedal, N. Czink, A. Paier, F. Tufvesson, and A. F. Molisch, "Path loss modeling for vehicle-to-vehicle communications," *IEEE Trans. Veh. Technol.*, vol. 60, no. 1, pp. 323–328, Jan. 2011.

[16] A. Theodorakopoulos, P. Papaioannou, T. Abbas, and F. Tufvesson, "A geometry based stochastic model for MIMO V2V channel simulation in cross-junction scenario," in *Proc. IEEE 13th Int. Conf. ITS Telecommun. (ITST)*, Nov. 2013, pp. 290–295.

[17] T. Abbas, L. Bernado, A. Thiel, C. Mecklenbrauker, and F. Tufvesson, "Radio channel properties for vehicular communication: Merging lanes versus urban intersections," *IEEE Veh. Technol. Mag.*, vol. 8, no. 4, pp. 27–34, Dec. 2013.

[18] P. Liu, B. Ai, D. W. Matolak, R. Sun, and Y. Li, "5-GHz vehicle-to-vehicle channel characterization for example overpass channels," *IEEE Trans. Veh. Technol.*, vol. 65, no. 8, pp. 5862–5873, Aug. 2016.

[19] T. Abbas, L. Bernado, A. Thiel, C. F. Mecklenbrauker, and F. Tufvesson, "Measurements based channel characterization for vehicle-to-vehicle communications at merging lanes on highway," in *Proc. IEEE 5th Int. Symp. Wireless Veh. Commun. (WiVeC)*, Jun. 2013, pp. 1–5.

[20] C. Li *et al.*, "Impact of soundproof walls on V2V communication in urban viaduct scenarios at 5.9 GHz band," presented at the IEEE 28th Annu. Int. Symp. Pers., Indoor, Mobile Radio Commun. (PIMRC), Montreal, QC, Canada, Oct. 2017.

[21] M. Pätzold, *Mobile Radio Channels*, 2nd ed. New York, NY, USA: Wiley, 2011.

[22] A. Molisch, *Wireless Communications*, 2nd ed. New York, NY, USA: Wiley, 2011.

[23] R. He, Z. Zhong, B. Ai, G. Wang, J. Ding, and A. F. Molisch, "Measurements and analysis of propagation channels in high-speed railway viaducts," *IEEE Trans. Wireless Commun.*, vol. 12, no. 2, pp. 794–805, Feb. 2013.

[24] R. He, Z. Zhong, B. Ai, J. Ding, Y. Yang, and A. F. Molisch, "Short-term fading behavior in high-speed railway cutting scenario: Measurements, analysis, and statistical models," *IEEE Trans. Antennas Propag.*, vol. 61, no. 4, pp. 2209–2222, Apr. 2013.

[25] K. P. Burnham and D. R. Anderson, *Model Selection and Multimodel Inference: A Practical Information-Theoretic Approach*. New York, NY, USA: Springer, 2003.

[26] X. Chen, "Using Akaike information criterion for selecting the field distribution in a reverberation chamber," *IEEE Trans. Electromagn. Compat.*, vol. 55, no. 4, pp. 664–670, Aug. 2013.

[27] U. G. Schuster and H. Bolcskei, "Ultrawideband channel modeling on the basis of information-theoretic criteria," *IEEE Trans. Wireless Commun.*, vol. 6, no. 7, pp. 2464–2475, Jul. 2007.

[28] S. Wyne, A. P. Singh, F. Tufvesson, and A. F. Molisch, "A statistical model for indoor office wireless sensor channels," *IEEE Trans. Wireless Commun.*, vol. 8, no. 8, pp. 4154–4164, Aug. 2009.

[29] X. H. Mao, Y. H. Lee, and B. C. Ng, "Statistical modeling of signal variation for propagation along a lift shaft," *IEEE Antennas Wireless Propag. Lett.*, vol. 9, no. 1, pp. 752–755, 2010.

[30] *Weibull Distribution*. Accessed: Jan. 5, 2018. [Online]. Available: https://en.wikipedia.org/wiki/Weibull_distribution

[31] *Nakagami Distribution*. Accessed: Jan. 8, 2018. [Online]. Available: https://en.wikipedia.org/wiki/Nakagami_distribution

[32] A. Goldsmith, *Wireless Communications*, 1st ed. New York, NY, USA: Cambridge Univ. Press, 2005.

[33] C. Fang *et al.*, "Indoor-indoor and indoor-outdoor propagation trial results at 2.6 GHz," in *Proc. IEEE Loughborough Antennas Propag. Conf.*, Nov. 2013, pp. 1–4.

[34] D. W. Matolak, I. Sen, W. Xiong, and N. T. Yaskoff, "5 GHz wireless channel characterization for vehicle to vehicle communications," in *Proc. IEEE MILCOM*, Oct. 2005, pp. 3016–3022.

[35] A. F. Molisch, F. Tufvesson, J. Karedal, and C. Mecklenbrauker, "Propagation aspects of vehicle-to-vehicle communications—An overview," in *Proc. IEEE Radio Wireless Symp. (RWS)*, Jan. 2009, pp. 179–182.

[36] H. El-Sallabi, M. Abdallah, J.-F. Chamberland, and K. Qaraqe, "A statistical model for delay domain radio channel parameter affected with extreme values," in *Proc. IEEE Int. Symp. Antennas Propag. (ISAP)*, Dec. 2014, pp. 165–166.

[37] G. S. Dahman, R. J. C. Bultitude, and R. H. M. Hafez, "Identifying and modelling multipath clusters in propagation measurement data," in *Proc. IEEE Veh. Technol. Conf. Fall*, Sep. 2010, pp. 1–5.

[38] F. J. Massey, Jr., "The Kolmogorov–Smirnov test for goodness of fit," *J. Amer. Stat. Assoc.*, vol. 46, no. 253, pp. 68–78, 1951.

[39] L. Bernado, T. Zemen, F. Tufvesson, A. F. Molisch, and C. F. Mecklenbrauker, "Delay and doppler spreads of nonstationary vehicular channels for safety-relevant scenarios," *IEEE Trans. Veh. Technol.*, vol. 63, no. 1, pp. 82–93, Jan. 2014.

[40] O. Renaudin, V.-M. Kolmonen, P. Vainikainen, and C. Oestges, "Wideband measurement-based modeling of inter-vehicle channels in the 5-GHz band," *IEEE Trans. Veh. Technol.*, vol. 62, no. 8, pp. 3531–3540, Oct. 2013.

[41] S. Kozono, "Received signal-level characteristics in a wide-band mobile radio channel," *IEEE Trans. Veh. Technol.*, vol. 43, no. 3, pp. 480–486, Aug. 1994.

[42] G. L. Stüber, *Principles of Mobile Communication*, 2nd ed. Norwell, MA, USA: Kluwer, 2001.

[43] J. Kunisch and J. Pamp, "Wideband car-to-car radio channel measurements and model at 5.9 GHz," in *Proc. IEEE Veh. Technol. Conf. VTC-Fall*, Sep. 2008, pp. 1–5.

[44] T. S. Rappaport, *Wireless Communications: Principles and Practice*, 2nd ed. Englewood Cliffs, NJ, USA: Prentice-Hall, 2002.

[45] N. Perpinias, A. Palaios, J. Riihijärvi, and P. Mähönen, "Impact of the path loss model on the spatial structure of shadow fading," in *Proc. IEEE Int. Conf. Commun.*, Jun. 2014, pp. 5871–5877.

CHANGZHEN LI was born in Jining, Shandong, China, in 1991. He received the B.S. and M.S. degrees in engineering from the Wuhan University of Technology, China, in 2013 and 2017, respectively, where he is currently pursuing the Ph.D. degree in traffic information engineering and control with the School of Automation. His main research interests include vehicle-to-vehicle communication, radio channel measurement, and modeling under complex driving environments.

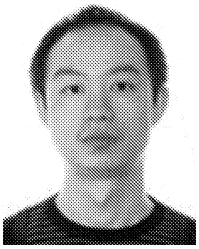

KUN YANG received the M.S. degree from the University of Agder, Norway, in 2007, and the Ph.D. degree from NTNU, Norway, in 2013. He joined the Wireless Devices and Systems Group, University of Southern California, and the Communications Theory Group, France, as a Visitor, in 2011 and 2012, respectively. He is currently leading the National Project on 5G Maritime Communication in Norway. His current research interests include radio channel measurement and modeling, Maritime broadband, massive multi-in multi-out, and millimeter-wave technologies.

JUNYI YU (M'17) was born in Zibo, Shandong, China, in 1988. He received the master's degree in engineering from the Wuhan University of Technology, Hubei, China, in 2013, where he is currently pursuing the Ph.D. degree in engineering with the School of Automation. His main research interests include wireless channel measurement and modeling, maritime informatization, vehicle-to-vehicle channel estimation, and massive multi-in multi-out technologies.

FANG LI was born in Heze, China, in 1990. She received the B.S. and M.S. degrees in engineering from the Wuhan University of Technology, China, in 2010 and 2013, respectively, where she is currently pursuing the Ph.D. degree in traffic control and information engineering. Her main research interests are vehicle-to-vehicle radio channel measurements and modeling.

YISHUI SHUI received the B.S. degree in communication engineering and the M.S. degree in communication and information system engineering from the Wuhan University of Technology, Wuhan, China, in 2010 and 2013, respectively, where he is currently pursuing the Ph.D. degree in information engineering. His main research interests are intelligent optimization algorithms and vehicle-to-vehicle radio channel measurements and modeling.

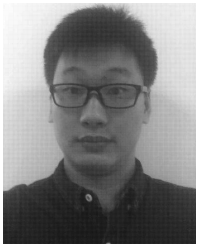

FUXING CHANG was born in Xinyang, China, in 1988. He received the master's degree in communication engineering from Guizhou University, Guiyang, in 2015. He is currently pursuing the Ph.D. degree from the Wuhan University of Technology, Wuhan, China. Since 2015, he has been a Teaching Assistant with the School of Information Engineering, Wuhan University of Technology. His main areas of research are numerical analysis of measurement data and modeling of wireless propagation channels.

WEI CHEN (M'06–SM'17) was born in Wuhan, China, in 1963. He received the Ph.D. degree in information and communication engineering from the Huazhong University of Science and Technology, Wuhan, China, in 2005. He is currently a Professor and a Doctoral Supervisor with the School of Automation, Wuhan University of Technology. His current research interests include channel measurement and modeling, massive multi-in multi-out technology, millimeter-wave technologies, satellite navigation system theory and technology application, and intelligent traffic control systems.

Prof. Chen is a member of the Communications and Navigation Standardization Technical Committee of the Ministry of Transport of China, a member of the Academic Committee on Communications and Navigation of the China Institute of Navigation, and a Senior Member of the China Electronics Society.